Structural analysis of urinary light chains and proteomic analysis of hyaline tubular casts in light chain associated kidney disorders

Thomas Reiter [1], **Daniela Knafl** [1], **Hermine Agis** [2], **Karl Mechtler** [3], **Ludwig Wagner** [Corresp., 1], **Wolfgang Winnicki** [1]

[1] Department of Medicine III, Division of Nephrology and Dialysis, Medical University of Vienna, Vienna, Austria

[2] Department of Medicine I, Division of Oncology, Medical University of Vienna, Vienna, Austria

[3] ProtChem Facility, IMP-IMBA, Research Institute of Molecular Pathology, Vienna, Austria

Corresponding Author: Ludwig Wagner
Email address: ludwig.wagner@meduniwien.ac.at

Background: Monoclonal overproduction of kappa and/or lambda light chains might result in renal light chain deposition disease. Light chain associated cast nephropathy and renal AL-amyloidosis represent two further pathologies going along with monoclonal gammopathy of renal significance and multiple myeloma. While cast nephropathy often manifests with acute kidney injury, AL-amyloidosis is rather accompanied with chronic kidney disease.

Methods: Urine samples were collected from 17 patients with multiple myeloma or monoclonal gammopathy. The urine sediment was stained for cast morphology by H/E and light chain immunofluorescence. Following micro-selection of casts under microscope, proteomic analysis of casts was performed by mass spectrometry. Sucrose gradient sedimentation was employed and light chain architecture examined by immunoblotting. Uromodulin was measured by ELISA in sucrose gradient fractions.

Results: Urinary casts were observed of about 30 μm in diameter by H/E staining and under immunofluorescence microscopy. Casts with a diameter of 20 μm were observed as a novel variant. Proteome analysis showed that in addition to the expected light chain variants produced by the malignant clone of plasma cells, also histones such as H2B and cathepsin B were contained. Uromodulin was not detectable in urinary casts of all patients. All eleven patients with lambda light chains showed predominant dimerized light chains in the urine immunoblot. Six patients with kappa light chains presented with predominantly monomeric forms of light chains in the immunoblot. The densitometric evaluated ratio of lambda dimers vs. monomers was significantly higher (2.12 ± 0.75) when compared with the ratio of kappa dimers vs. monomers (0.64 ± 0.47), p=0.00001. Aggregates of light chains separated in part into denser sucrose fractions.

Conclusion: This work on urinary casts and light chains demonstrates that hyaline tubular casts represent a complex formation of protein-protein aggregates with histones and cathepsin B identified as novel cast components. Apart from the proteomic composition of the casts, also the formation of the light chains and aggregates is of relevance. Dimerized light chains, which are typical for lambda paraproteins, might be less dialyzable than monomeric forms and may therefore identify patients less responsive to high cut-off dialysis.

Structural analysis of urinary light chains and proteomic analysis of hyaline tubular casts in light chain associated kidney disorders

5 Thomas Reiter[1], Daniela Knafl[1], Hermine Agis[2], Karl Mechtler[3], Ludwig Wagner[1], Wolfgang

6 Winnicki[1]

8 [1] Department of Medicine III, Division of Nephrology and Dialysis, Medical University of

9 Vienna, Austria

10 [2] Department of Medicine I, Division of Oncology, Medical University of Vienna, Austria

11 [3] ProtChem Facility, IMP-IMBA, Research Institute of Molecular Pathology, Vienna, Austria.

14 Corresponding Author:

15 Ludwig Wagner,

16 Waehringer Guertel 18-20, 1090 Vienna, Austria

17 Email adress: ludwig.wagner@meduniwien.ac.at

21 **Abstract**

22 **Background:** Monoclonal overproduction of kappa and/or lambda light chains might result in

23 renal light chain deposition disease. Light chain associated cast nephropathy and renal AL-

24 amyloidosis represent two further pathologies going along with monoclonal gammopathy of

25 renal significance and multiple myeloma. While cast nephropathy often manifests with acute

26 kidney injury, AL-amyloidosis is rather accompanied with chronic kidney disease.

27 **Methods:** Urine samples were collected from 17 patients with multiple myeloma or monoclonal

28 gammopathy. The urine sediment was stained for cast morphology by H/E and light chain

29 immunofluorescence. Following micro-selection of casts under microscope, proteomic analysis

30 of casts was performed by mass spectrometry. Sucrose gradient sedimentation was employed and

31 light chain architecture examined by immunoblotting. Uromodulin was measured by ELISA in

32 sucrose gradient fractions.

33 **Results:** Urinary casts were observed of about 30 μm in diameter by H/E staining and under

34 immunofluorescence microscopy. Casts with a diameter of 20 μm were observed as a novel

35 variant. Proteome analysis showed that in addition to the expected light chain variants produced

36 by the malignant clone of plasma cells, also histones such as H2B and cathepsin B were

37 contained. Uromodulin was not detectable in urinary casts of all patients.

38 All eleven patients with lambda light chains showed predominant dimerized light chains in the

39 urine immunoblot. Six patients with kappa light chains presented with predominantly monomeric

40 forms of light chains in the immunoblot. The densitometric evaluated ratio of lambda dimers vs.

41 monomers was significantly higher (2.12 ± 0.75) when compared with the ratio of kappa dimers

42 vs. monomers (0.64 ± 0.47), p=0.00001. Aggregates of light chains separated in part into denser

43 sucrose fractions.

44   **Conclusion:** This work on urinary casts and light chains demonstrates that hyaline tubular casts

45   represent a complex formation of protein-protein aggregates with histones and cathepsin B

46   identified as novel cast components. Apart from the proteomic composition of the casts, also the

47   formation of the light chains and aggregates is of relevance. Dimerized light chains, which are

48   typical for lambda paraproteins, might be less dialyzable than monomeric forms and may

49   therefore identify patients less responsive to high cut-off dialysis.

50

51 **Introduction**

52 Renal manifestation of multiple myeloma or elevated free light chains due to monoclonal

53 gammopathy frequently manifest in light chain associated kidney disorders with different forms

54 of deposits in renal compartments (Leung et al. 2019). The spectrum of renal complications

55 associated with paraproteins is heterogeneous, with two major categories corresponding to the

56 properties of the underlying B-cell clone. The first group is always associated with a high tumor

57 mass and in this context cast nephropathy is of particular significance. The second group

58 includes all patients with renal symptoms associated with a nephrotoxic monoclonal

59 immunoglobulin as clonal proliferative disorder and is defined as monoclonal gammopathy of

60 renal significance (MGRS) (Leung et al. 2012). Depending on results of immunofluorescence

61 and electron microscopy, MGRS-associated diseases may include immunoglobulin light chain

62 (AL) amyloidosis, monoclonal fibrillary glomerulonephritis (GN), immunotactoid GN,

63 cryoglobulinaemic GN, light-chain proximal tubulopathy, crystal storing histiocytosis,

64 monoclonal immunoglobulin deposition disease as well as proliferative glomerulonephritis and

65 monoclonal immunoglobulin deposits (Leung et al. 2019; Leung et al. 2012).

66 Monoclonal overproduction of light chains by plasma cells represents the origin of the renal

67 pathology. Since the publication of these studies nephrologists and oncologists have learned

68 much in this direction (Hutchison et al. 2011; Manohar et al. 2018). Diagnostic procedures have

69 been extended to include measurement of free light chain ratio in the serum, protein

70 electrophoresis in serum and urine, immunofixation in serum and urine, bone marrow and renal

71 biopsy (Leung 2016), whereas free light chain measurement in the urine is not recommended

72 (Bradwell et al. 2003; Dispenzieri et al. 2009; Leung et al. 2019). Urine sediment testing for

73   presence of urinary casts is simple, noninvasive and not harmful to patients and is included in

74   any diagnostic workup for patients with acute kidney injury (AKI).

75   Tubular cast formation has been attributed to specific non-covalent binding of light chains with

76   uromodulin proteins (Huang & Sanders 1997). This is provoked when the proximal tubular

77   epithelia are overloaded with high concentrations of kappa or lambda light chains which under

78   normal conditions are reabsorbed by proximal tubular epithelial cells through a multiligand

79   endocytic receptor complex (Ying et al. 2012). This receptor complex is assumed to be

80   constituted out of megalin (Klassen et al. 2005) and cubilin (Batuman et al. 1998) as silencing of

81   both genes resulted in ablation of free light chain induced uptake and toxicity in human renal

82   proximal tubule epithelial cells (Ying et al. 2012). The primary structure of the monoclonal free

83   light chain which results in a defined isoelectric point of the protein has much influence on the

84   morphology and location of the light chain disease (Abraham et al. 2003) such as cast

85   nephropathy (Cogne et al. 1991; Stevens 2000), AL-amyloidosis (Enqvist et al. 2007; Omtvedt et

86   al. 2000; Stevens 2000) or monoclonal immunoglobulin deposition disease (del Pozo Yauner et

87   al. 2008; Deret et al. 1997). However, individual patient-specific predisposing factors and

88   medication (Holland et al. 1985; Ying & Sanders 1998) might represent similar important

89   players in renal disease morphology and progression. In this respect, secretion and reabsorption

90   of other proteins and pharmacotherapeutic compounds (Luque et al. 2017) in urine appear to

91   have a significant effect on cast formation. There is currently evidence that the human urinary

92   proteome consists of more than 1000 individual protein fragments shaded or secreted into the

93   urine (Liu et al. 2012; Marimuthu et al. 2011). It has already been reported that renal casts have

94   variable hematoxylin/eosin staining intensities and might contain further compounds beyond

95   uromodulin and light chain (Luque et al. 2017).

96   These previous studies have motivated us to investigate the protein constituents of nephron

97   obstructing tubular casts through specific staining and micro-selection of these casts in the

98   urinary sediment. Casts are usually observed in the distal tubule, however, there is evidence that

99   they are also found in the proximal tubule and even in glomeruli (Start et al. 1988). In this study

100   analyzing urinary secreted casts, there are indications that thin casts might even originate from

101   the loop of Henle. Proteome analysis of these casts might help to shed further light on genesis

102   and potential treatment strategies in the clinical work up of patients with deranged free light

103   chain composition in urine. Free light chain dimerization or multimerization may influence

104   clearance properties when high cut-off membrane dialysis is intended. Therefore, in addition to

105   staining of urine sediment and proteomic analysis of casts, immunoblotting of urinary light

106   chains was an important focus of this study.

107 **Materials & Methods**

108 **Urine sediment**

109 Morning urine samples were collected from 17 patients with multiple myeloma or monoclonal

110 gammopathy of renal/undetermined significance. Demographics, clinical course of the patients

111 and their predominant paraprotein are depicted in **Table 1**. After centrifugation of the urine at

112 3000 g for 10 minutes, the supernatant was frozen at -80°C for later use in fluid analysis. The

113 pellet was re-suspended in 2.5 mL cell culture media (RPMI 1640 containing 10% calf serum)

114 and 100μL were applied to the funnel of a Shandon cyto-centrifuge. Following a spin at 1200

115 RPM for 3 minutes cytoslides were air dried for at least two hours and then either immediately

116 processed as described below or wrapped in aluminum foil and frozen at -25°C for further

117 analysis.

118

119 **Hematoxylin/Eosin staining** was carried out as used in routine hematology staining of blood

120 smears. Slides were covered in Depex mounting media and a cover slip was applied for

121 microscopic observation.

122

123 **Immunofluorescence for anti kappa/lambda staining** (confocal microscopy) was carried out

124 after fixation in acetone for 4 minutes. The cell and cast containing area was surrounded by a fat

125 pen (Dako) and the staining area was rewetted using PBS. For kappa/lambda staining goat

126 (diluted 1:10000, A0191 and A0193 from Dako) or rabbit anti human kappa/lambda polyclonal

127 antibody (Ab) (P0212, Dako) was applied (1:5000 in PBS) and incubated for two hours at room

128 temperature following two washes in PBS each for 10 minutes, the donkey anti goat or goat anti

129 rabbit (Alexa 488, dilution 1:1000 in PBS) was applied for 1 hour at room temperature. Before

130   washing the slide 20 µL of DAPI solution was spotted onto the Ab containing area. Following

131   the final wash Vetashield mounting media and cover slip were applied and the slides were

132   recorded under a Zeiss invert confocal microscope using ZEN program for picture recording.

133

134   **Urinary cast isolation**

135   Urine sediment generated as described above was air dried from patients presenting with AL-

136   amyloidosis and cast nephropathy or presenting with cast nephropathy alone. Cytopreparations

137   were viewed under phase contrast light microscope (Labovert FS, Leitz, Germany) and

138   individual casts were picked using the tip of specifically gas flame pulled glass Pasteur pipettes

139   under microscopic observation. Five casts were placed into a 400 µL PCR tube containing

140   10bµL PBS. This represented the work up starting material for proteome analysis.

141

142   **Substructural fractionation on a sucrose gradient**

143   Cells and cell nuclei and large aggregates were pelleted by centrifugation at 1500 RPM. Five

144   hundred µL of resultant supernatant containing cast fragments and micro-aggregates and

145   exosomes were loaded on to a discontinuous sucrose gradient in Ultra-clear centrifuge tubes

146   (Beckman, 344062) at 4°C. Following two hours centrifugation at 40000 RPM using an SW60

147   rotor in an L-80 ultracentrifuge the gradient was immediately fractionated in 200 µL aliquots

148   using a peristaltic pump starting at the bottom of the tube. Individual fractions were subjected to

149   immunoblotting using antibodies for kappa and lambda light chains (Dako as above) and

150   aquaporin 1 (AQP1, Millipore).

151

152   **Immunoblotting**

153   Twenty µL of individual fractions of urine were loaded onto a 12% SDS PAGE gel and run

154   under denaturing conditions. Following the transfer onto nitrocellulose the proteins were stained

155   using kappa and lambda specific antibodies (Dako) as well as Ab against AQP1 (Millipore). The

156   specific protein staining was developed by HRP labeled goat anti rabbit affinity purified

157   antibodies (Dako). After each staining procedure the blot was washed using TPBS for 10

158   minutes twice. Chemiluminescence reagent was applied to the blot which was visualized using

159   Fusion software at the luminescence recorder (Fusion Fx, Vilber Lourmat). Pictures were further

160   processed using Photoshop version 6. Densitometric evaluation of individual signals of dimers

161   vs. monomers were performed using the Fusion software (Fusion Fx, Vilber Lourmat).

162

163   **Uromodulin ELISA test**

164   Uromodulin concentration was measured in the same sucrose density gradient fractions as used

165   for immunoblotting by a commercially available ELISA assay (BioVendor, Czech Republic).

166   The Elisa was performed as suggested in the company's test manual. In brief, fractions were

167   diluted in sample dilution buffer and incubated together with the standard series. Following the

168   incubation with biotinylated detection antibody and streptavidin-HRP conjugate the signal was

169   developed with TMB substrate and read by an ELISA reader. Concentrations were calculated

170   according the standard curve. The detection range of the ELISA assay is 0.5 to 25 ng/mL.

171

172   **Mass spectrometry**

173   **NanoLC-MS Analysis:** Trypsin digestion was carried out in solution and resultant peptides were

174   purified on a C18 column before injection into the UltiMate 3000 RSLC nano HPLC system

175   (Thermo Fisher Scientific, Amsterdam, Netherlands). This was connected to a Q Exactive HF mass

176   spectrometer (Thermo Fisher Scientific, Bremen, Germany) with a Proxeon nanospray source

177   (Thermo Fisher Scientific, Odense, Denmark). Initial loading was carried out onto a trap column

178   (Thermo Fisher Scientific, Amsterdam, Netherlands, PepMap C18, 5 mm × 300 μm ID, 5 μm

179   particles, 100 Å pore size) at a flow rate of 25 μL min-1 using 0.1% TFA as mobile phase. This

180   column was moved in line with the analytical column (Thermo Fisher Scientific, Amsterdam,

181   Netherlands, PepMap C18, 500 mm × 75 μm ID, 2 μm, 100 Å) following a 10 minute flow.

182   Peptides were eluted by a binary 1h gradient with a flow rate of 230 nL min-1. The applied gradient

183   for starting represented: 98% A (water/formic acid, 99.9/0.1, v/v) and 2% B

184   (water/acetonitrile/formic acid, 19.92/80/0.08, v/v/v). Over a period of 60 minutes B was increased

185   to 35% and over the next 5 minutes B was further increased up to 90% and was kept in a plateau

186   for 5 minutes. Within the next 2 minutes the gradient was returned back to 98% A and 2% B. This

187   was the setting for equilibration at 30°C.

188   The mass spectrometer was set to data-dependent mode in full scan (m/z range 380-1650, nominal

189   resolution of 120,000, target value 3E6) followed by MS/MS scans of the 10 most abundant ions.

190   MS/MS spectra were obtained using normalized collision energy of 27%, isolation width of 2 m/z,

191   resolution of 30,000 and the target value was set to 1E5. Precursor ions selected for fragmentation

192   were read at dynamic exclusion list for 20 sec. Additionally, the minimum AGC target was set to

193   2E4. The intensity threshold was calculated to be 8E4.

194

195   **Data Processing protocol and peptide identification:**

196   The Proteome Discoverer (version 2.3.0.523, Thermo Scientific) was fed with RAW-data files.

197   The generated MS/MS spectra have been searched using MSAmanda v2.0.0.9849 (Dorfer et al.

198   2014). RAW-files were searched against the SwissProt human database (20,169 sequences;

199 11315,794 residues). The search parameters were: peptide mass tolerance ±5 ppm as well as the

200 fragment mass tolerance was limited to 0.03 Da. Missed cutting sites were 2. The resultant output

201 was filtered to 1 % false discovery rate using again Thermo Proteome Discoverer. Peptide area

202 under the curve was quantified using IMP-apQuant (Doblmann et al. 2019).

203 **Statistical analyses**

204 We present quotients as means ± standard deviation (SD). Differences of lambda and kappa

205 dimer vs. monomer ratio were analyzed with paired t-test. Data management and analysis was

206 conducted by Microsoft Excel (© Microsoft, Redmont, WA). The statistical testing performed

207 was two-sided and a p-value ≤ 0.05 was considered significant.

208

209 **Ethics approval and consent to participate**

210 This study involves human participants. Urine samples were obtained from adult study

211 participants and/or their legal guardians older than 18 years who have given written informed

212 consent. All methods of experiments involving human participants were carried out according to

213 relevant guidelines. All experimental protocols involving human participants received approval

214 of the Ethics Committee of the Medical University of Vienna (EK 1043/2016).

215

216

217

218

219

220 **Results**

221 **Cast morphology and constituent analysis**

222 Hematoxylin/Eosin staining of tubular casts revealed various staining intensities as well as

223 colour variation. Colour variation results from different contents, which either are more

224 basophilic or acidophilic depending on constituents. As demonstrated in **Figure 1A,C,D** three

225 casts are more eosinophilic when compared to one in **Figure 1B** that shows a fainter staining.

226 The thinner cast at **Figure 1C** is originating from a different stretch of the nephron than the other

227 cast fragments, such as the the loop of Henle. Three tubular cells are incorporated in this thin

228 cast.

229 In order to further study the constituents of tubular casts we sought for the incorporation of light

230 chain components. As already reported in earlier work tubular casts contain the light chain (LC)

231 paraprotein such as also measured in serum. As shown in **Figure 2A and 2B** the lambda light

232 chain is incorporated at the tubular cast which has a thinner diameter at the left side upward

233 directed end when compared with the other part. This picture further confirms the assumption

234 that casts can originate from thinner stretches of the nephron.

235 Analysis of casts by electron microscopy has identified various fine structures in previous studies

236 (Uribe-Uribe & Herrera 2006) and the most dominant variant was represented by the hyaline

237 form, however, the biochemical proteinaceous constituents of hyaline casts in light chain

238 associated kidney disorders has not been the subject of investigation before. Only uromodulin

239 was documented as light chain interaction partner. Therefore we sought by mass spectrometry to

240 analyze the proteome of isolated urinary casts from patient 14 who had no detectable uromodulin

241 in the sucrose density fractionation. In these experiments we identified the patient's lambda LC

242 and histones in particular H2B sub-variants **(Table 2)** as a dominant additional constituents of

243 the cast proteome. It is of interest that a urinary protease such as cathepsin B was also contained

244 in this complex **(Table 2)**. In repeated proteome analyses (n=3) H2 variants were similarly

245 highly present. Depending on the cast type chosen for analysis more or less cellular proteins

246 were recovered. However, this study was focused on hyaline casts. Of particular note is the

247 observation that as shown in **(Supplementary Figure 1)** patient 14 had received

248 immunomodulatory therapy 2.5 days before the onset of AKI stage 3 according to KDIGO. His

249 urine sediment was filled with hyaline casts. The liberation of histones from apoptotic plasma

250 cells and the filtration into the urine might have represented the main provocation of cast

251 formation in the renal tubules as uromodulin was not detectable. His lambda light chain analysis

252 in the density gradient fractions **(Figure 3A)** showed to some extent presence of aggregated LC

253 signals in density fractions 6-10 representing most likely complexes but there was almost no

254 presence of LCs in exosome containing fractions 2-6. Presence of exosomes was verified by

255 immunoblotting of the same fractions with Ab against AQP1 a tubular cell membrane protein

256 **(Figure 3B)**. By a second approach using urine SDS PAGE analysis and immunoblotting lambda

257 LCs appeared predominantly as dimers in urine and made up 78% in the densitometric analysis

258 **(Figure 4, lane 14)**. No amyloid deposition had been observed in the kidney biopsy of this

259 patient although the duration of disease had been lasting for already 5 years **(Table 1)**. The

260 patient underwent high cut-off dialysis and as demonstrated in **Supplementary Figure 1** his

261 renal function improved.

262

263 **Analysis of urinary light chain structure**

264 As already documented in earlier work not the concentration but rather the structure and

265 morphology represents the underlying cause for manifestation of renal light chain disease. For

266   this reason we analyzed the light chain dimerization in 17 myeloma or monoclonal gammopathy

267   patients **(Table 1)**. As demonstrated in **Figure 4** patients positive for lambda LCs showed

268   patterns with higher quantities of LC dimers than monomers. Furthermore, eight patients out of

269   11 positive for lambda LC developed CKD stages 4-5 according to KDIGO (**Table 1**). Patients

270   3, 8, 9, 10, 13 and 14 were highly positive for lambda dimers in the immunoblots **(Figure 4)**.

271   Dimerization of lambda LC could be entirely resolved into monomers by adding DDT as

272   reducing agent in the sample buffer **(Figure 4B).**

273   Patients positive for kappa LCs showed patterns with higher quantities of LC monomers than

274   dimers (**Figure 5**). The densitometric analysis evaluated ratio of lambda dimers vs. monomers

275   was significantly higher (2.12 ± 0.75) when compared with the ratio of kappa dimers vs.

276   monomers (0.64 ± 0.47), p=0.00001.

277   We further intended to elaborate the light chain aggregates or complex formation resulting in

278   renal light chain disease by density gradient centrifugation in patients 13, 14 and 15. In the urine

279   sediment of amyloidosis patient 13 the light chain was found in both the soluble urine proteins

280   (**Figure 6A**, fractions 11-14) and to a lesser extent in the membrane fractions (**Figure 6A,** lanes

281   1-4**)**. Membrane exosome fractions were identified by AQP1 blotting of the same fractions

282   **(Figure 6B).** This was similar for patient 15 despite the fact that his disease was linked to kappa

283   LC which was going along with AKI stage 3 **(Figure 7A)**. Membrane fractions represented by

284   lanes 1-4 containing exosomes and cast particles were identified by presence of AQP1 (**Figure**

285   **7B**).

286   The Uromodulin protein (UMOD) has been shown earlier to represent the binding partner for

287   LCs in forming casts. In this study we did not find uromodulin protein in the casts of patient 14,

288   which was confirmed by absence in sucrose gradient density fractions and urine. In contrast,

289   there was a small peak concentration in heavy membrane fraction 2 in patients 13 and 15 **(Figure**

290   **6C and Figure 7C)**. This fractions corresponded with presence of exosomes and cast fragments

291   in the gradient sedimentation experiments. Fractions 11-14 correspond to soluble molecules in

292   urine. In patients 13 and 15 urine uromodulin concentration was high (**Figure 6C and Figure**

293   **7C).**

294 Discussion

295 This study investigates hyaline cast constituents and factors involved in cast formation as well as

296 urine light chain multimeric conformation. It documents that casts of thinner diameter than

297 assumed can be observed in light chain disease which might originate from the loop of Henle.

298 Selective cast harvesting by micromanipulation under microscope observation for proteome

299 analysis revealed histones as major constituents of casts together with the light chain present as

300 serum and urine paraprotein. Rather unexpectedly, cathepsin B was also found among the

301 dominant cast constituents. In addition, all patients with lambda light chains showed

302 dimerization of urine light chains in the immunoblot and were more likely to develop

303 amyloidosis and chronic kidney disease.

304 Secretion of light chains has been shown in previous studies to predominantly occur as

305 monomers *in vitro* (Dul et al. 1996) but this does not have to apply to multiple myeloma patients

306 *in vivo*. In our study patients positive for lambda LCs showed patterns with higher quantities of

307 LC dimers than monomers in urine immunoblotting. In contrast, patients positive for kappa LCs

308 showed patterns with higher quantities of LC monomers than dimers. This may represent an

309 important observation for potential clinical treatment options such as high cut-off dialysis

310 (Bridoux et al. 2017; Finkel 2014). The much smaller monomeric forms might represent better

311 candidates for clearance through dialysis, whereas dimers may require longer dialysis and may

312 be less cleared from plasma. It would therefore be reasonable to test patients for LC structure and

313 size morphology to assess the potential benefit of high cut-off hemodialysis.

314 Earlier work (Korbet & Schwartz 2006; Luque et al. 2017) and this study confirm that cast

315 formation and amyloid fibrilogenesis (Kim et al. 2000) represent complex physicochemical and

316 biochemical processes (Radamaker et al. 2019). Interaction of electrostatic charges between

317   proteins such as uromodulin (Huang & Sanders 1997) together with nephron-specific biological

318   processes such as incorporation of exosomes shaded from tubular epithelial brush border are of

319   importance. In addition, proteins filtered through the glomerulum and not reabsorbed by the

320   proximal tubular epithelia seem to represent important players in hyaline cast formation.

321   In our cast experiments histones getting liberated from apoptotic cells during chemotherapy,

322   representing small positively charged molecules of 13-17 kDa, which are filtered through the

323   glomerular membrane, seem to have acted as partners for LCs to form hyaline casts. In this

324   situation no uromodulin concentrations in the urine could be measured of the patient having

325   undergone immunomodulatory therapy and AKI. Thus it has to be suggested, that cast formation

326   might be induced by various proteins and biological compounds (Luque et al. 2017) beyond

327   uromodulin. Hence, novel considerations in management of cast nephropathy might be important

328   (Manohar et al. 2018; Ying et al. 2012).

329   It has been documented earlier that Bence Jones protein and amyloid fibril generated out of LCs

330   are C-terminally cleaved (Enqvist et al. 2009; Terry et al. 1973). In this line the abundant

331   presence of Cathepsin B in hyaline casts represents a protease known for cleaving C-terminal

332   parts in the process of activation/inactivation of various biologically active compounds (Kumar

333   et al. 2018). It is therefore of interest that Cathepsin B might be involved in proteolytic

334   processing of the C-terminal part of the cast components in particular the LCs. Cathepsin B is

335   most likely involved in proteolytic digestion and thereby mobilization of casts from the site of

336   tubular obstruction. It is of note that in fraction 14 of Figure 7A (soluble urine proteins) the light

337   chain dimer is of reduced size probably because of cleavage, which must have been achieved by

338   urine contained proteases such as cathepsins.

339   Brush border specific proteins are contained in the hyaline casts isolated from the urine sediment

340   in individual specimens. Some of the patient derived hyaline casts contained cells to various

341   extent. This demonstrates that cast formation at a specific stretch of the nephron causes injury to

342   tubular epithelial cells or cells subsequently loosen from the basal membrane when the tubule

343   dilates proximal to the part, which had been obstructed by the cast. Proteases incorporated (such

344   as cathepsin) might contribute to cast liberation because of proteolytic digestion and thereby

345   shrinkage of the cast.

346   We found kappa and lambda LCs in the heavy fractions of the sucrose gradient at densities

347   where exosomes and cast fragments were expected. This revealed that LCs are present in

348   microsomes where AQP1 is present or it represents cast fragments.

349   The molecular size of LC in serum must have an important impact on its clearance by the

350   glomerulum and by high cut-off dialysis membranes. LC testing using urine immunoblotting to

351   determine the molecular size of LC proteins appears to be an important option for evaluating

352   whether a patient could benefit from high cut-off dialysis treatment. Lambda-positive patients

353   known for the presence of higher polymers (Sallee & Burtey 2019), as confirmed in this study,

354   may not be good candidates for LC clearance through high-cut off dialysis membranes.

355   The main limitation of this study is that no clinically available quantitative methods are available

356   for measurement of LC dimers versus monomers, therefore this study uses semi-quantitative

357   methods. Casts for proteomic analysis could not be isolated from all patients and not all patients

358   underwent renal biopsy. Due to the limits of proteomic databases, only well-known peptide

359   sequences can be detected by proteome analysis. In respect of clinical treatment regimens this

360   structural analysis of casts and light chains is preliminary and focused on a small sample size.

361   This may encourage clinical researchers at the same time to conduct studies in larger patient

362 groups on different treatment regimens, in particular on lambda/kappa light-chain associated

363 kidney disorders. It is of note, that in our study for the first time proteomic analysis was

364 performed on micro-selected cast structures.

365

366 **Conclusions**

367 This study demonstrates that hyaline tubular casts represent a complex formation of protein-

368 protein aggregates with histones and cathepsin B identified as novel cast components. Apart

369 from the proteomic cast composition, the formation of light chains and aggregates is of particular

370 significance. Dimerized light chains typical for lambda paraproteins might be less dialyzable

371 than monomeric forms. Therefore, testing for light chain structure may select patients who are

372 more likely to benefit from dialysis using high cut-off membranes, but clinical trials are required

373 to confirm this.

374 **References**

375 Abraham RS, Geyer SM, Price-Troska TL, Allmer C, Kyle RA, Gertz MA, and Fonseca R.

376   2003. Immunoglobulin light chain variable (V) region genes influence clinical

377   presentation and outcome in light chain-associated amyloidosis (AL). *Blood* 101:3801-

378   3808. 10.1182/blood-2002-09-2707

379 Batuman V, Verroust PJ, Navar GL, Kaysen JH, Goda FO, Campbell WC, Simon E, Pontillon F,

380   Lyles M, Bruno J, and Hammond TG. 1998. Myeloma light chains are ligands for cubilin

381   (gp280). *The American journal of physiology* 275:F246-254.

382   10.1152/ajprenal.1998.275.2.F246

383 Bradwell AR, Carr-Smith HD, Mead GP, Harvey TC, and Drayson MT. 2003. Serum test for

384   assessment of patients with Bence Jones myeloma. *Lancet* 361:489-491. Doi

385   10.1016/S0140-6736(03)12457-9

386 Bridoux F, Carron PL, Pegourie B, Alamartine E, Augeul-Meunier K, Karras A, Joly B, Peraldi

387   MN, Arnulf B, Vigneau C, Lamy T, Wynckel A, Kolb B, Royer B, Rabot N, Benboubker

388   L, Combe C, Jaccard A, Moulin B, Knebelmann B, Chevret S, and Fermand JP. 2017.

389   Effect of High-Cutoff Hemodialysis vs Conventional Hemodialysis on Hemodialysis

390   Independence Among Patients With Myeloma Cast Nephropathy: A Randomized

391   Clinical Trial. *JAMA* 318:2099-2110. 10.1001/jama.2017.17924

392 Cogne M, Preud'homme JL, Bauwens M, Touchard G, and Aucouturier P. 1991. Structure of a

393   monoclonal kappa chain of the V kappa IV subgroup in the kidney and plasma cells in

394   light chain deposition disease. *The Journal of clinical investigation* 87:2186-2190.

395   10.1172/JCI115252

396   del Pozo Yauner L, Ortiz E, Sanchez R, Sanchez-Lopez R, Guereca L, Murphy CL, Allen A,

397   Wall JS, Fernandez-Velasco DA, Solomon A, and Becerril B. 2008. Influence of the

398   germline sequence on the thermodynamic stability and fibrillogenicity of human lambda

399   6 light chains. *Proteins* 72:684-692. 10.1002/prot.21934

400   Deret S, Chomilier J, Huang DB, Preud'homme JL, Stevens FJ, and Aucouturier P. 1997.

401   Molecular modeling of immunoglobulin light chains implicates hydrophobic residues in

402   non-amyloid light chain deposition disease. *Protein engineering* 10:1191-1197.

403   Dispenzieri A, Kyle R, Merlini G, Miguel JS, Ludwig H, Hajek R, Palumbo A, Jagannath S,

404   Blade J, Lonial S, Dimopoulos M, Comenzo R, Einsele H, Barlogie B, Anderson K,

405   Gertz M, Harousseau JL, Attal M, Tosi P, Sonneveld P, Boccadoro M, Morgan G,

406   Richardson P, Sezer O, Mateos MV, Cavo M, Joshua D, Turesson I, Chen W, Shimizu K,

407   Powles R, Rajkumar SV, Durie BGM, and Grp IMW. 2009. International Myeloma

408   Working Group guidelines for serum-free light chain analysis in multiple myeloma and

409   related disorders. *Leukemia* 23:215-224. 10.1038/leu.2008.307

410   Doblmann J, Dusberger F, Imre R, Hudecz O, Stanek F, Mechtler K, and Durnberger G. 2019.

411   apQuant: Accurate Label-Free Quantification by Quality Filtering. *Journal of Proteome*

412   *Research* 18:535-541. 10.1021/acs.jproteome.8b00113

413   Dorfer V, Pichler P, Stranzl T, Stadlmann J, Taus T, Winkler S, and Mechtler K. 2014. MS

414   Amanda, a universal identification algorithm optimized for high accuracy tandem mass

415   spectra. *Journal of proteome research* 13:3679-3684. 10.1021/pr500202e

416   Dul JL, Aviel S, Melnick J, and Argon Y. 1996. Ig light chains are secreted predominantly as

417   monomers. *Journal of immunology* 157:2969-2975.

418   Enqvist S, Sletten K, Stevens FJ, Hellman U, and Westermark P. 2007. Germ line origin and

419   somatic mutations determine the target tissues in systemic AL-amyloidosis. *PloS one*

420   2:e981. 10.1371/journal.pone.0000981

421   Enqvist S, Sletten K, and Westermark P. 2009. Fibril protein fragmentation pattern in systemic

422   AL-amyloidosis. *The Journal of pathology* 219:473-480. 10.1002/path.2607

423   Finkel KW. 2014. Is high cut-off hemodialysis effective in myeloma kidney? *Seminars in*

424   *dialysis* 27:234-236. 10.1111/sdi.12210

425   Holland MD, Galla JH, Sanders PW, and Luke RG. 1985. Effect of urinary pH and diatrizoate on

426   Bence Jones protein nephrotoxicity in the rat. *Kidney international* 27:46-50.

427   Huang ZQ, and Sanders PW. 1997. Localization of a single binding site for immunoglobulin

428   light chains on human Tamm-Horsfall glycoprotein. *The Journal of clinical investigation*

429   99:732-736. 10.1172/JCI119218

430   Hutchison CA, Batuman V, Behrens J, Bridoux F, Sirac C, Dispenzieri A, Herrera GA,

431   Lachmann H, and Sanders PW. 2011. The pathogenesis and diagnosis of acute kidney

432   injury in multiple myeloma. *Nature reviews Nephrology* 8:43-51.

433   10.1038/nrneph.2011.168

434   Kim Y, Wall JS, Meyer J, Murphy C, Randolph TW, Manning MC, Solomon A, and Carpenter

435   JF. 2000. Thermodynamic modulation of light chain amyloid fibril formation. *The*

436   *Journal of biological chemistry* 275:1570-1574. 10.1074/jbc.275.3.1570

437   Klassen RB, Allen PL, Batuman V, Crenshaw K, and Hammond TG. 2005. Light chains are a

438   ligand for megalin. *Journal of applied physiology* 98:257-263.

439   10.1152/japplphysiol.01090.2003

440 Korbet SM, and Schwartz MM. 2006. Multiple myeloma. *Journal of the American Society of*

441 *Nephrology : JASN* 17:2533-2545. 10.1681/ASN.2006020139

442 Kumar A, Daitsh Y, Ben-Aderet L, Qiq O, Elayyan J, Batshon G, Reich E, Maatuf YH, Engel S,

443 and Dvir-Ginzberg M. 2018. A predicted unstructured C-terminal loop domain in SIRT1

444 is required for cathepsin B cleavage. *Journal of cell science* 131. 10.1242/jcs.214973

445 Leung N. 2016. To biopsy or not to biopsy, that is the question in myeloma cast nephropathy.

446 *Nephrology, dialysis, transplantation : official publication of the European Dialysis and*

447 *Transplant Association - European Renal Association* 31:1-3. 10.1093/ndt/gfv294

448 Leung N, Bridoux F, Batuman V, Chaidos A, Cockwell P, D'Agati VD, Dispenzieri A, Fervenza

449 FC, Fermand JP, Gibbs S, Gillmore JD, Herrera GA, Jaccard A, Jevremovic D, Kastritis

450 E, Kukreti V, Kyle RA, Lachmann HJ, Larsen CP, Ludwig H, Markowitz GS, Merlini G,

451 Mollee P, Picken MM, Rajkumar VS, Royal V, Sanders PW, Sethi S, Venner CP,

452 Voorhees PM, Wechalekar AD, Weiss BM, and Nasr SH. 2019. The evaluation of

453 monoclonal gammopathy of renal significance: a consensus report of the International

454 Kidney and Monoclonal Gammopathy Research Group. *Nature Reviews Nephrology*

455 15:45-59. 10.1038/s41581-018-0077-4

456 Leung N, Bridoux F, Hutchison CA, Nasr SH, Cockwell P, Fermand JP, Dispenzieri A, Song

457 KW, and Kyle RA. 2012. Monoclonal gammopathy of renal significance: when MGUS is

458 no longer undetermined or insignificant. *Blood* 120:4292-4295. 10.1182/blood-2012-07-

459 445304

460 Liu X, Shao C, Wei L, Duan J, Wu S, Li X, Li M, and Sun W. 2012. An individual urinary

461 proteome analysis in normal human beings to define the minimal sample number to

462   represent the normal urinary proteome. *Proteome science* 10:70. 10.1186/1477-5956-10-

463   70

464 Luque Y, Louis K, Jouanneau C, Placier S, Esteve E, Bazin D, Rondeau E, Letavernier E,

465   Wolfromm A, Gosset C, Boueilh A, Burbach M, Frere P, Verpont MC, Vandermeersch

466   S, Langui D, Daudon M, Frochot V, and Mesnard L. 2017. Vancomycin-Associated Cast

467   Nephropathy. *Journal of the American Society of Nephrology : JASN* 28:1723-1728.

468   10.1681/ASN.2016080867

469 Manohar S, Nasr SH, and Leung N. 2018. Light Chain Cast Nephropathy: Practical

470   Considerations in the Management of Myeloma Kidney-What We Know and What the

471   Future May Hold. *Current hematologic malignancy reports* 13:220-226. 10.1007/s11899-

472   018-0451-0

473 Marimuthu A, O'Meally RN, Chaerkady R, Subbannayya Y, Nanjappa V, Kumar P, Kelkar DS,

474   Pinto SM, Sharma R, Renuse S, Goel R, Christopher R, Delanghe B, Cole RN, Harsha

475   HC, and Pandey A. 2011. A comprehensive map of the human urinary proteome. *Journal*

476   *of proteome research* 10:2734-2743. 10.1021/pr2003038

477 Omtvedt LA, Bailey D, Renouf DV, Davies MJ, Paramonov NA, Haavik S, Husby G, Sletten K,

478   and Hounsell EF. 2000. Glycosylation of immunoglobulin light chains associated with

479   amyloidosis. *Amyloid : the international journal of experimental and clinical*

480   *investigation : the official journal of the International Society of Amyloidosis* 7:227-244.

481   10.3109/13506120009146437

482 Radamaker L, Lin YH, Annamalai K, Huhn S, Hegenbart U, Schonland SO, Fritz G, Schmidt M,

483   and Fandrich M. 2019. Cryo-EM structure of a light chain-derived amyloid fibril from a

484   patient with systemic AL amyloidosis. *Nature communications* 10:1103.

485   10.1038/s41467-019-09032-0

486   Sallee M, and Burtey S. 2019. Myeloma cast nephropathy: the dusk of high cutoff

487   haemodialysis. *The Lancet Haematology* 6:e174-e176. 10.1016/S2352-3026(19)30044-4

488   Start DA, Silva FG, Davis LD, D'Agati V, and Pirani CL. 1988. Myeloma cast nephropathy:

489   immunohistochemical and lectin studies. *Modern pathology : an official journal of the*

490   *United States and Canadian Academy of Pathology, Inc* 1:336-347.

491   Stevens FJ. 2000. Four structural risk factors identify most fibril-forming kappa light chains.

492   *Amyloid : the international journal of experimental and clinical investigation : the*

493   *official journal of the International Society of Amyloidosis* 7:200-211.

494   Terry WD, Page DL, Kimura S, Isobe T, Osserman EF, and Glenner GG. 1973. Structural

495   identity of Bence Jones and amyloid fibril proteins in a patient with plasma cell dyscrasia

496   and amyloidosis. *The Journal of clinical investigation* 52:1276-1281. 10.1172/JCI107295

497   Uribe-Uribe NO, and Herrera GA. 2006. Ultrastructure of Tubular Casts. *Ultrastructural*

498   *Pathology* 30:159-166. 10.1080/01913120600689749

499   Ying WZ, Allen CE, Curtis LM, Aaron KJ, and Sanders PW. 2012. Mechanism and prevention

500   of acute kidney injury from cast nephropathy in a rodent model. *The Journal of clinical*

501   *investigation* 122:1777-1785. 10.1172/JCI46490

502   Ying WZ, and Sanders PW. 1998. Dietary salt regulates expression of Tamm-Horsfall

503   glycoprotein in rats. *Kidney international* 54:1150-1156. 10.1046/j.1523-

504   1755.1998.00117.x

505

Figure 1

H/E stained casts on cyto-slide preparations obtained from a patient with lambda light chain myeloma.

Urine sediment obtained in the context of AKI stage 3 revealed multiple casts. The average cast diameter comprised about 30 μm **(A, B, D)**. Considerable thinner cast containing tubular cells most likely originating from a thinner part of the nephron (**C**). Pale staining tubular cast originating from the distal tubule **(B)**.
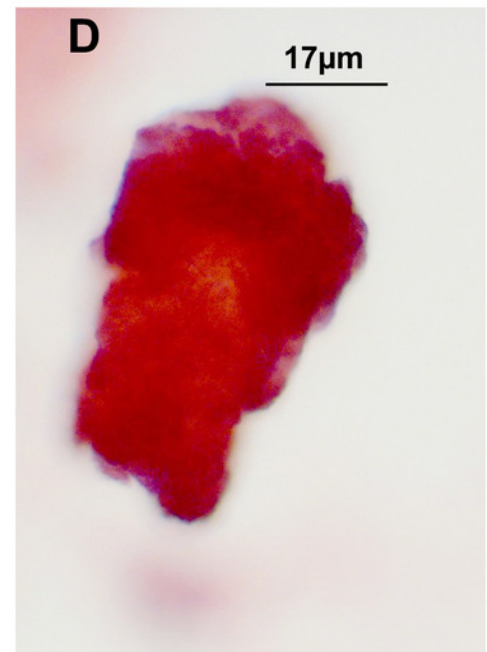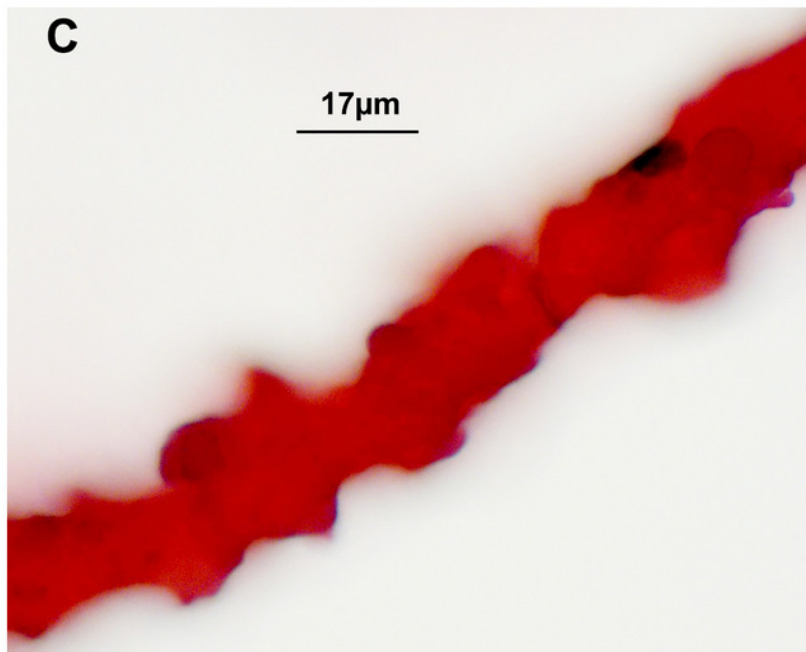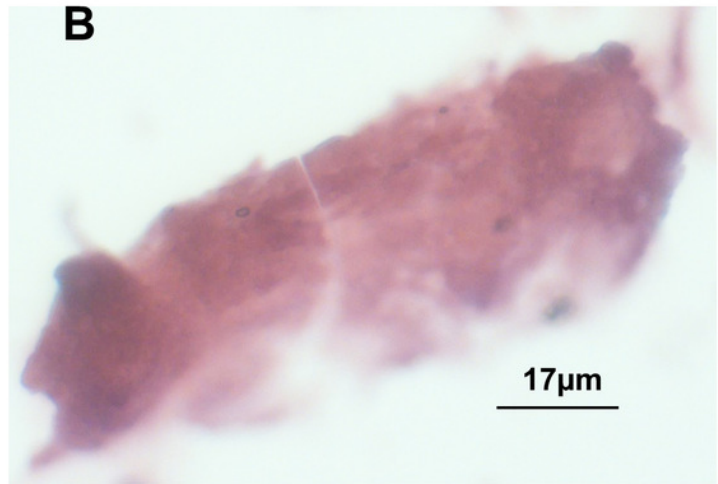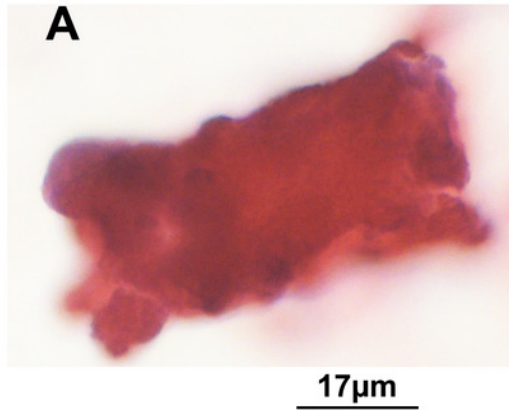
Figure 2

Immunofluorescence staining of renal tubular casts. Various staining intensity for lambda light chain of tubular casts.

The cast is bent and shows a conical structure with the thinner part directed upwards. This

has a diameter of about 23 μm whereas most other casts show a diameter of about 30 μm

(A). Casts contain remnants of tubular cells with condensed nuclear DNA **(B)**.
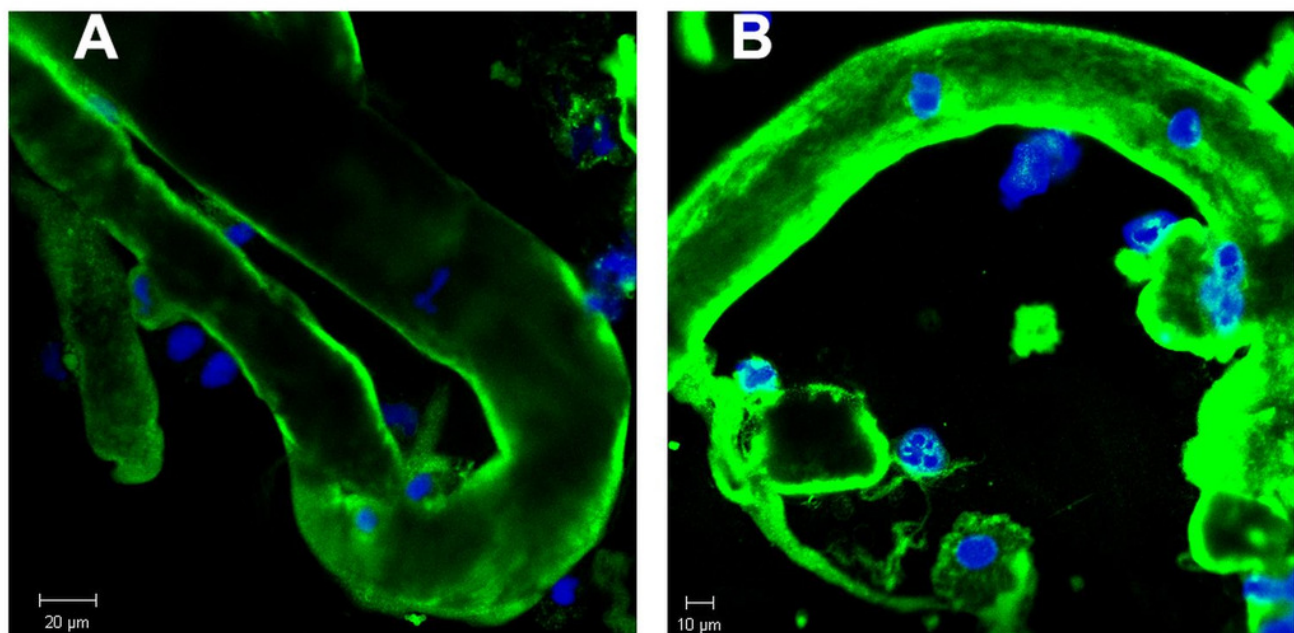
Figure 3

Sucrose density gradient separation of urine of patient 14 containing cast fragments, exosomes and micro-aggregates.

The centrifuged (40000 g for 2 hours) sucrose gradient (500 µL urine containing cast fragments and micro-aggregates) was fractionated into 14 individual fractions. Individual fractions were loaded onto a 12% SDS PAGE gel, transferred to nitrocellulose and developed for lambda light chains **(A)**. The same fractions were reprocessed and blotted for aquaporin 1 (AQP1) as a marker protein for heavy exosomes entering the dense sucrose layers such as in fractions 2-6 **(B)**.
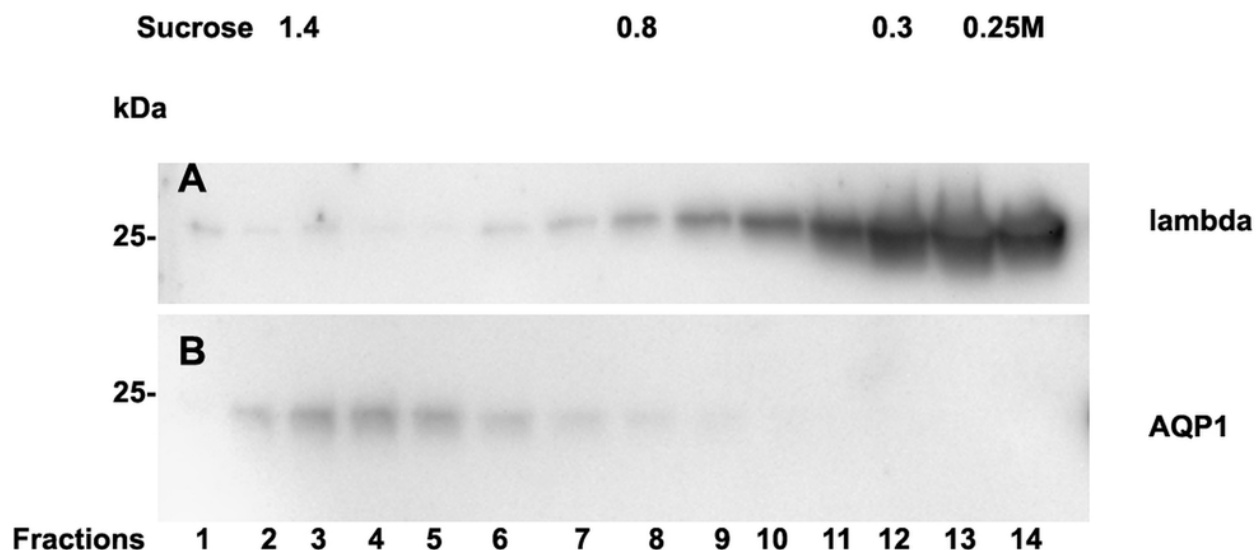
Figure 4

Urine lambda LC immunoblotting.

Twenty µL urine were loaded onto a 12% SDS PAGE gel and run under non-reducing conditions. The gel was blotted onto nitrocellulose and developed using a lambda LC-specific Ab **(A)**. The clinical course of the patients and predominant LCs are given in **Table 1**. The same fractions were loaded onto a 12% SDS PAGE gel and run under denaturing and reducing conditions. The gel was blotted onto nitrocellulose which was developed with the lambda LC-specific Ab. Only monomeric forms of LCs were depicted (**B)**. Patients are numbered at the bottom of the picture in accordance to **Table 1**. The molecular weight is shown on the left side and light chain multimerization status is shown on the right. Ig stands for immunoglobulin.
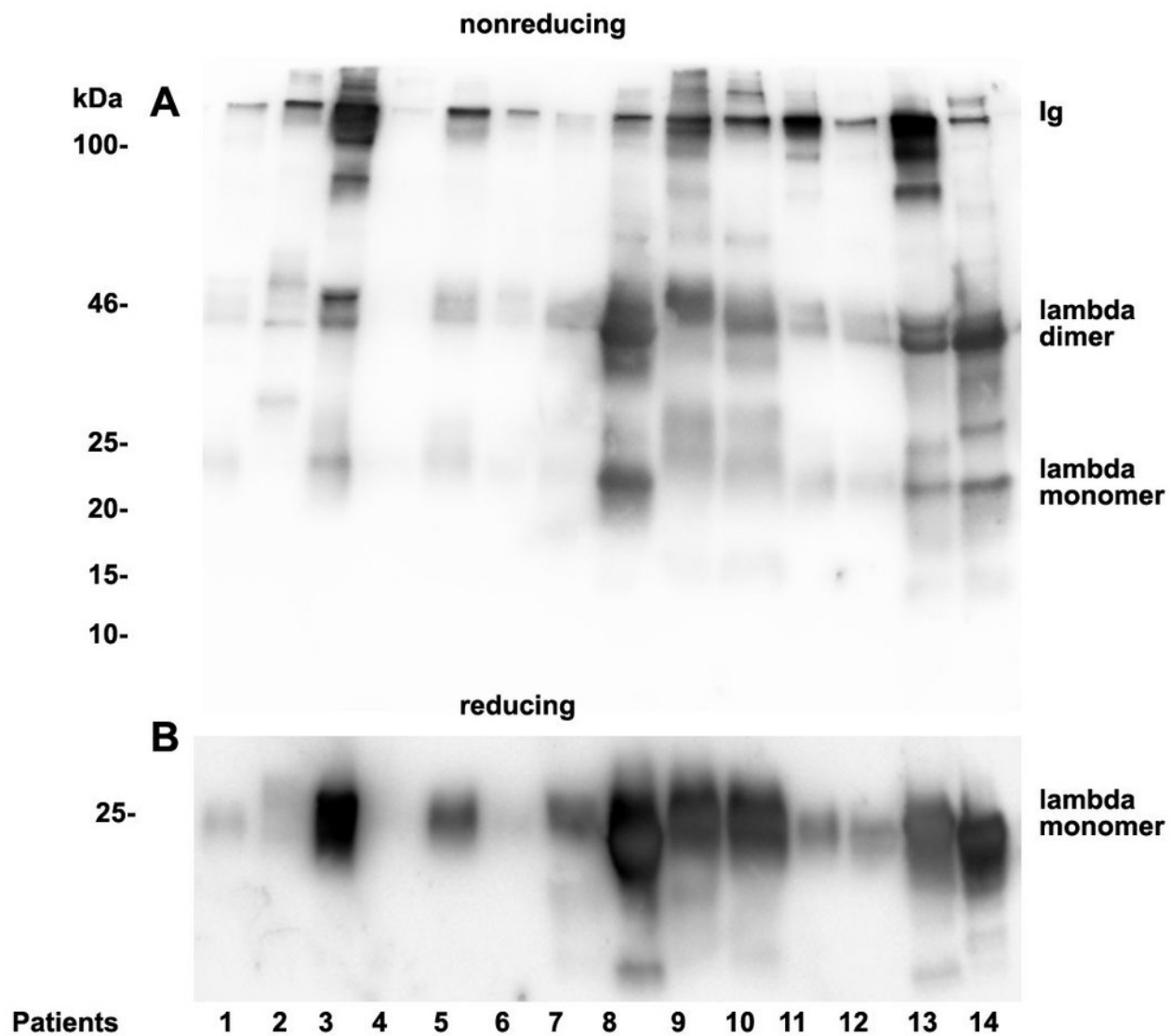
Figure 5

Urine kappa LC immunoblotting

Twenty µL urine were loaded onto a 12% SDS PAGE gel and run under non-reducing conditions. The gel was blotted onto nitrocellulose and developed using a kappa LC-specific Ab (**A**). The patients' clinical conditions and predominant LC are illustrated in **Table 1**. The same fractions were loaded onto a 12% SDS PAGE gel and run under reducing and denaturing conditions. The gel was blotted onto nitrocellulose which was developed with the kappa LC-specific Ab. Only monomeric forms of LCs were depicted (**B**). Patients are numbered at the bottom of the picture in accordance to **Table 1**. The molecular weight is shown on the left side and light chain multimerization status is shown on the right. Ig stands for immunoglobulin.

nonreducing

A

kDa

100-

46-

25-

20-

15-

10-

Ig

kappa
dimer

kappa
monomer

reducing

B

25-

kappa
monomer
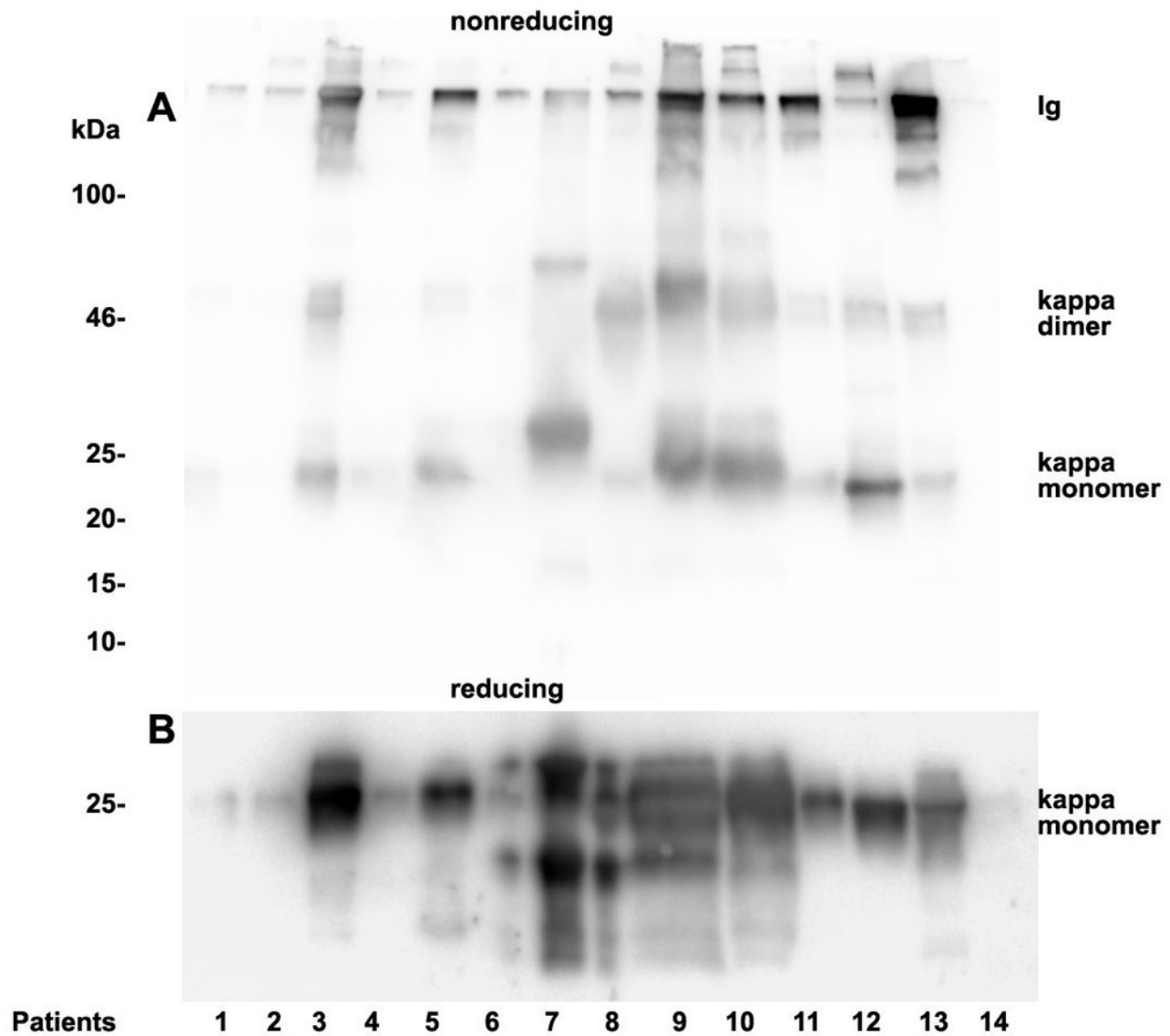
Patients   1   2   3   4   5   6   7   8   9   10   11   12   13   14
Figure 6

Sucrose density gradient separation of 500 µL urine of patient 13 containing cast fragments, micro-aggregates and exosomes.

The centrifuged (40000 g for 2 hours) sucrose gradient was fractionated into 14 individual fractions which were loaded onto a 12% SDS PAGE gel, transferred to nitrocellulose and developed for lambda light chains. Molecular weight is depicted on the left, lambda dimers and lambda monomers are indicated at the right, fraction numbering is indicated at the bottom and sucrose density at the top **(A)**. The same fractions were tested for AQP1 **(B)** and for uromodulin concentration by ELISA **(C)**.

Sucrose   1.4   0.8   0.3   0.25M

kDa

A

100-

46-   lambda
                                                                        dimer

25-   lambda
                                                                        monomer

25-   AQP1

B

Fractions   1   2   3   4   5   6   7   8   9   10   11   12   13   14

C

6000

4000

UMOD ng/ml

2000

Fractions   1   2   3   4   5   6   7   8   9   10   11   12   13   14
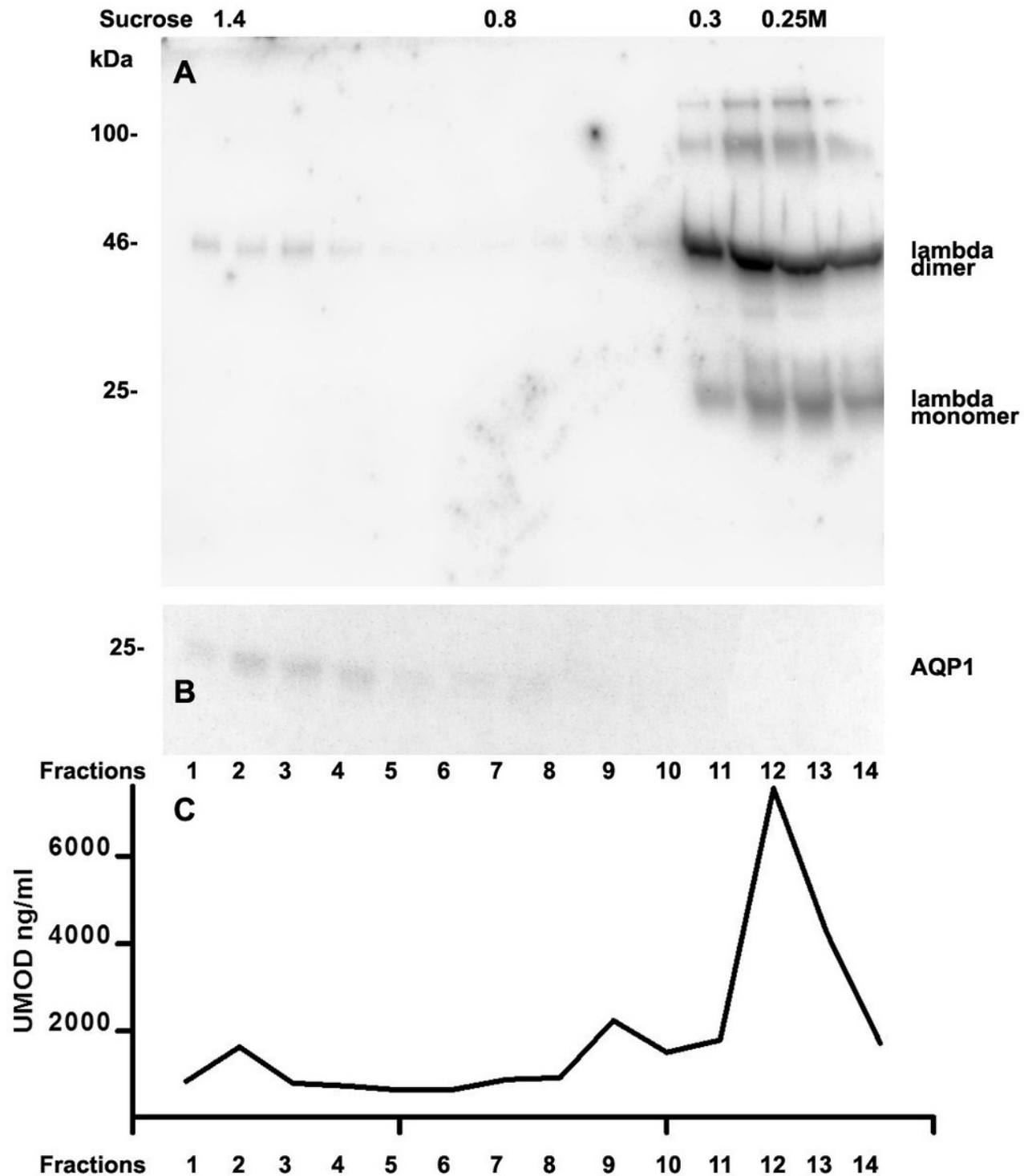
Figure 7

Sucrose density gradient separation of urine containing cast fragments, micro-aggregates and exosomes from patient 15.

The centrifuged (40000 g for 2 hours) sucrose gradient (500 μL urine containing cast fragments and micro-aggregates) was fractionated into 14 individual fractions. Individual fractions were loaded onto a 12% SDS PAGE gel, transferred to nitrocellulose and developed for kappa light chains. The legend to kappa monomers and dimers is indicated on the right **(A)**. The same fractions were tested for AQP1 **(B)** and for UMOD by ELISA **(C)**.

Sucrose   1.4   0.8   0.3   0.25M

kDa

100-

A

46-   kappa
                                                             dimer

25-   kappa
                                                             monomer

B   AQP1

25-

Fractions   1   2   3   4   5   6   7   8   9   10   11   12   13   14

C

Fractions   1   2   3   4   5   6   7   8   9   10   11   12   13   14
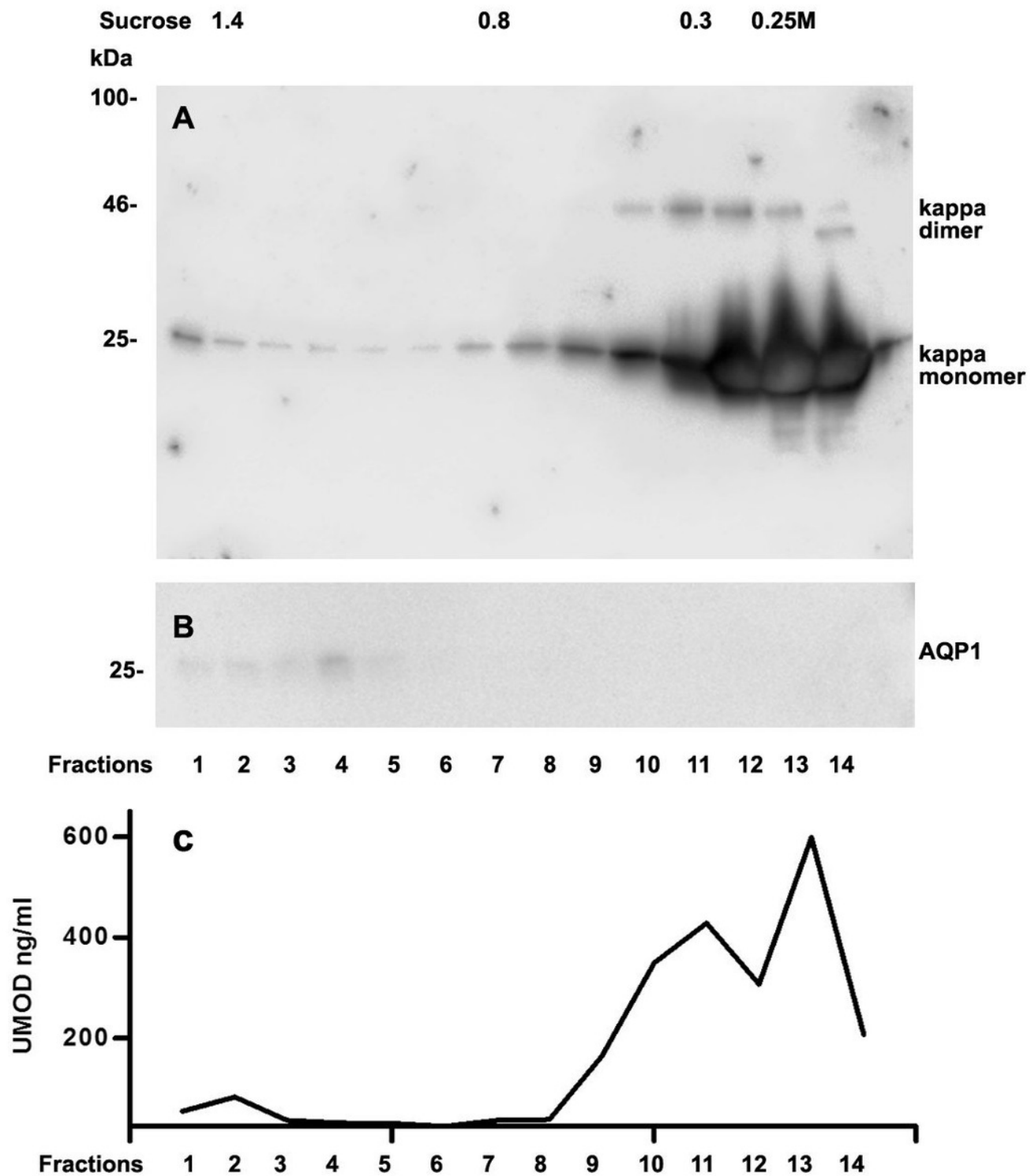
Demographics, clinical characteristics and specification of light chain associated kidney disorder.

Abbreviations: AKI, acute kidney injury; CKD, chronic kidney disease; f, female; ID, identification; LC, light chain; LCCN, Light-chain cast nephropathy; LCPT, light-chain proximal tubulopathy; m, male; MGRS, monoclonal gammopathy of renal significance; MGUS, monoclonal gammopathy of undetermined significance; MM, multiple myeloma; nd, not done; ns, not shown; sCr, serum creatinine; pos, positive; TMA, thrombotic microangiopathy; U:P/C, urinary protein/creatinine ratio.

° extrarenal manifestation of amyloidosis, * at time of diagnosis.

Previous clinical therapy: 1: Bortezomib, 2: Thalidomide, 3: Cyclophosphamide, 4: Dexamethasone, 5: Carfilzomib, 6: Lenalidomid, 7: Daratumumab, 8: Rituximab.

ID	Age (years)	Gender	LC	Hematological Classification	Renal Histology	Disease Duration (years)	sCr* (mg/dL)	Urinary Cast	CKD/AKI	U:P/C (mg/g)	Previous Therapy	Illustration
1	69	f	λ	MM	LCPT	1	1.24	0	1	112	1,3	Fig 4&5 / lane1
2	76	f	λ	MM	nd	10	0.81	0	1	81	5,6	Fig 4&5 / lane2
3	76	m	λ	MGRS	LCPT	4	1.2	0	4	1714		Fig 4&5 / lane3
4	87	f	κ	MM	nd	6	1.07	0	2	1	8	Fig 4&5 / lane4
5	63	f	κ	MM	nd	6	0.61	0	1	274	1,3,4	Fig 4&5 / lane5
6	49	m	κ	MM °	nd	1	1.12	0	2	214	1,4,7	Fig 4&5 / lane6
7	75	m	κ	MM	nd	0	2.12	0	5	697	3	Fig 4&5 / lane7
8	57	f	λ	MM °	LCCN	5	5.33	0	5	767	1,2,4	Fig 4&5 / lane8
9	62	m	λ	MGUS	nd	0	0.84	0	4	476		Fig 4&5 / lane9
10	63	m	λ	MGUS	nd	0	1.05	0	4	273		Fig 4&5 / lane10
11	67	f	λ	MM °	TMA	4	2.02	0	4	222	1,4	Fig 4&5 / lane11
12	80	m	κ	MM	nd	0	1.04	0	2	126	2,4,5	Fig 4&5 / lane12
13	67	f	λ	MM °	LCCN, LCPT, AL-amyloidosis	1	1.59	pos	5	5631	1,7	Fig 4&5 / lane13; Fig 6
14	55	m	λ	MM	LCCN	5	1.22	pos	4/3	4781	1	Fig 4&5 / lane14; Fig3; Sup. Fig 1
15	59	m	κ	MM	LCCN	1	6.58	pos	3/3	5561	1,2	Fig 7
16	75	m	λ	MM °	LCCN, AL-amyloidosis	0	4.2	pos	5	4643		ns
17	48	m	λ	MM °	nd	7	0.92	0	1	38	1,2,4	ns

Proteome analysis using NanoLC-MS Analysis of 5 individual casts selected under microscopic observation by micromanipulation.

Five hyaline casts were picked from a cytoslide and analytically processed. Abundance of peptides is calculated as area under the curve (Norm. Area) of highly specific peptide peaks. Shown is one analysis out of three.

Accession	Description	MW[kDa]	Norm. Area
P0CG04.1	Immunoglobulin lambda constant 1	11,34	**3,92E+07**
P0DOX8.1	Immunoglobulin lambda-1 light chain	22,82	**2,29E+07**
B9A064.2	Immunoglobulin lambda-like polypeptide 5	23,05	**2,11E+07**
P0CF74.1	Immunoglobulin lambda constant 6	11,27	**1,96E+07**
P0DOY3.1	Immunoglobulin lambda constant 3	11,26	**7,19E+06**
P07858.3	Cathepsin B	37,80	**1,49E+06**
Q16778.3	Histone H2B type 2-E	13,91	**1,02E+06**
Q5QNW6.3	Histone H2B type 2-F	13,91	**1,02E+06**
Q99879.3	Histone H2B type 1-M	13,98	**1,02E+06**
P33778.2	Histone H2B type 1-B	13,94	**1,02E+06**
P58876.2	Histone H2B type 1-D	13,93	**1,02E+06**
Q93079.3	Histone H2B type 1-H	13,88	**1,02E+06**
Q99880.3	Histone H2B type 1-L	13,94	**1,02E+06**
P62807.4	Histone H2B type 1-C/E/F/G/I	13,90	**1,02E+06**
Q8N257.3	Histone H2B type 3-B	13,90	**1,02E+06**
P23527.3	Histone H2B type 1-O	13,90	**1,02E+06**
Q99877.3	Histone H2B type 1-N	13,91	**1,02E+06**
P31151.4	Protein S100-A7	11,46	**9,34E+05**
Q96A08.3	Histone H2B type 1-A	14,16	**8,90E+05**
O00584.2	Ribonuclease T2	29,46	**7,65E+05**
P01834.2	Immunoglobulin kappa constant	11,76	**6,81E+05**
P01860.2	Immunoglobulin heavy constant gamma 3	41,26	**6,67E+05**
Q6ZVX7.1	F-box only protein 50	30,83	**6,25E+05**
Q5T749.1	Keratinocyte proline-rich protein	64,09	**5,34E+05**
P0DOX7.1	Immunoglobulin kappa light chain	23,36	**3,40E+05**
Q9H1E1.2	Ribonuclease 7	17,41	**2,86E+05**
Q05639.1	Elongation factor 1-alpha 2	50,44	**1,49E+05**
P68104.1	Elongation factor 1-alpha 1	50,11	**1,49E+05**
Q5VTE0.1	Putative elongation factor 1-alpha-like 3	50,15	**1,49E+05**
P00558.3	Phosphoglycerate kinase 1	44,59	**1,45E+05**